ACS Sustainable Chemistry & Engineering

Research Article

pubs.acs.org/journal/ascecg

Aqueous-Phase Synthesis of Copper Nanoparticles Using Organic Nanoparticles: Application of Assembly in Detection of Cr^{3+}

Ajnesh Singh,[†] Simanpreet Kaur,[‡] Amanpreet Kaur,[‡] Thammarat Aree,[§] Navneet Kaur,*[,‡] Narinder Singh,*[,†] and Mandeep Singh Bakshi[∥]

[†]Department of Chemistry, Indian Institute of Technology Ropar (IIT Ropar), Rupnagar, Panjab, India 140001

[‡]Centre for Nanoscience and Nanotechnology (UIEAST), Panjab University, Chandigarh, India 160014

[§]Department of Chemistry, Faculty of Science, Chulalongkorn University, Phyathai Rd., Pathumwan, Bangkok 10330, Thailand

[∥]Department of Chemistry, Wilfrid Laurier University, Waterloo, Ontario N2L 3C5, Canada

Supporting Information

ABSTRACT: A series of novel heterotripodal receptors were synthesized with potential cation binding sites. Their crystal structure revealed the presence of extensive intramolecular as well as intermolecular hydrogen bonding, which allowed them to process into organic nanoparticles (ONPs) in aqueous medium. The ONPs thus synthesized showed extraordinary ability for chromogenic recognition of Cu^{2+} ions, with the consequence that they could easily reduce Cu(II) into Cu(0) to produce copper nanocrystals (CuNCs) that grew on the surface of ONPs to generate hybrid nanomaterials, and were characterized by a number of studies. The hybrid NPs thus produced act as fluorescent probes for detection of Cr^{3+} in aqueous phase, whereas neither of its constituents (i.e., ONPs or CuNCs) showed this recognition behavior.

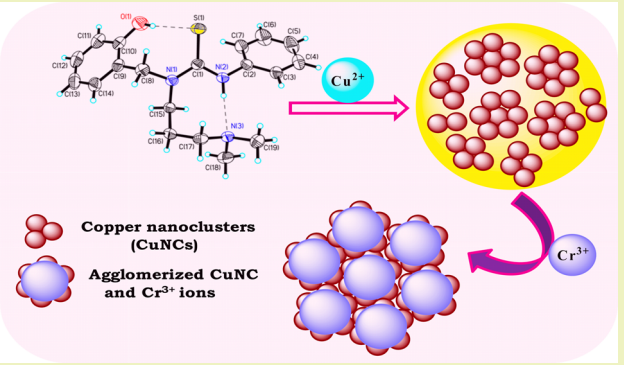

KEYWORDS: *Organic nanoparticles, Copper nanoclusters, Chromogenic studies, Chromium recognition*

INTRODUCTION

Tripodal ligands have been receiving a lot of attention for a long time as chemosensors because they provide three tunable pods for the optimum utilization of the binding sites for selective sensing and quantification of biologically important metal ions and anions.[1−5] The seminal work in this field includes recognition of sulfate by squaramide-based tripodal receptors,[6] triaminomethyl−triethylbenzene-based fluorescence turn-on tripodal sensor array for phosphates in blood serum,[7] sulfate recognition by hexaurea-based tripodal receptors,[8] star-shaped tripodal chemosensors for detection of aliphatic amines,[9] and many more in this direction.[10−14] However, most of these studies have been performed in organic solvents or in a certain ratio of water to other nonaqueous solvents that are commonly not referred to as environment friendly solvents. Sensing and recognition of important metal ions in pure aqueous phase is of great relevance to biologically as well as environmentally friendly analyses. Recent advances in the synthesis of organic nanoparticles (ONPs)[15−19] in aqueous medium find several applications in the development of chemosensors capable of detecting biologically, industrially, and environmentally important ions like Cu^{2+} in aqueous medium. Copper is of immense biological importance as it is the essential trace element for many biological processes and catalyst in many industrial processes, and at the same time, it is a significant environmental pollutant due to its extensive use.[20−23] In addition, excessive intake of copper can cause many gastrointestinal disturbances and kidney/liver damage.[24]

In the present work, we have developed[25−27] four receptors, **3**−**6** (Scheme 1), to look into the chemosensor properties of their ONPs. ONPs have been prepared simply by following the reprecipitation method and facilitated by extensive hydrogen bonding as discussed above. ONPs have always better advantages than their constituting monomeric tripod ligand molecules in view of their applications as drug release vehicles.[28−30] Among the ONPs of receptors **3**−**6**, receptor **3** has shown high selectively for Cu^{2+} ions in the presence of other biologically important ions. This selectivity is triggered by a strong redox process involving the reduction of Cu(II) into Cu(0) by receptor **3** molecules on the surface of their ONPs to produce copper nanoclusters (CuNCs). This is a rarely seen process where ONPs of an organic tripod ligand are involved in a single-step reduction process and show such a strong reducing behavior. To our knowledge, there are only few reports[31−36] related to the synthesis of CuNCs, whereas the present work is probably the first report on the synthesis of CuNCs using

Received: December 25, 2013
Revised: January 28, 2014
Published: February 2, 2014

Scheme 1. Receptors 1−6

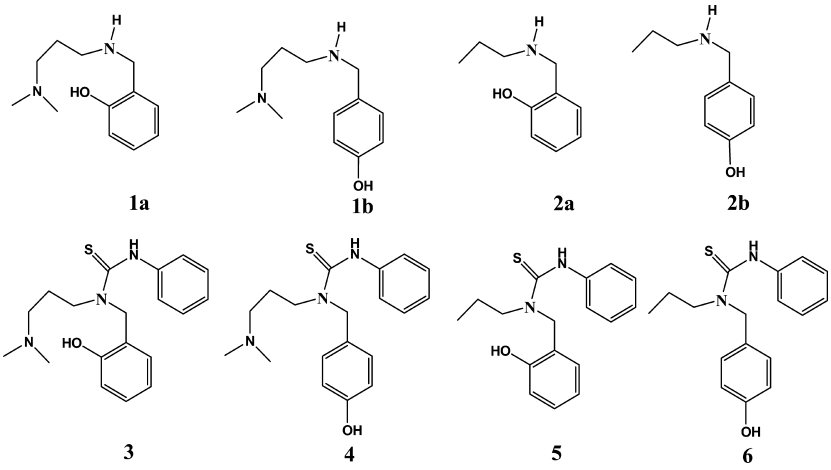

ONPs of a tripodal receptor in a simple one-pot synthetic process. Previous reports based on the synthesis of CuNCs are mainly focused on using polymers, proteins, DNA, dendrimers, and thiols[31−36] as templates, while the use of tripodal ligands opens up a new direction of one-step reduction synthesis of CuNCs. CuNCs have also wide applications in the fields of catalysis and antifungal and antibacterial agents; therefore, the use of tripodal receptors toward the synthesis of stable and biocompatible CuNCs with emission in the visible range is a step forward in the synthesis of organic−inorganic hybrid nanomaterials with great implications in environmental chemistry. In addition, CuNCs are also known[37,38] to exhibit localized surface plasmon resonance (SPR) in the visible region due to the collective resonance of their conduction band electrons just like Au and Ag NPs. Thus, ONPs−CuNCs hybrid materials are considered to be environmentally friendly materials with a precise ability to detect harmful Cr^{3+} ions.

EXPERIMENTAL SECTION

Materials and Methods. All chemicals were purchased from Sigma−Aldrich and were used without further purification. ^{1}H NMR and ^{13}C NMR spectra were recorded on an Avance-II (Bruker) instrument, which operated at 400 MHz for ^{1}H NMR and 100 MHz for ^{13}C NMR. Fourier transform infrared (FT-IR) spectra of dried compounds were measured on a Bruker Tensor 27 spectrophotometer using a KBr pellet technique. Elemental analyses were carried out on a Fisons instrument (Model EA 1108 CHNO). For cation recognition studies, the UV−vis absorption spectra were taken using dilute solutions in quartz cells (1 cm path length) on a Specord 250 Plus Analytikjena spectrometer. Steady-state and time-resolved fluorescence spectroscopy of ONPs suspensions were carried out by using PTI QuantaMaster and PicoMaster 2 TCSPC Lifetime fluorometer, respectively. Both instruments were equipped with a thermoelectrically temperature-controlled cell holder that measured the spectrum at a constant temperature within ±1 °C. The X-ray single-crystal studies were conducted on a Bruker X8 APEX II KAPPA CCD diffractometer. The particle size of NPs was determined with dynamic light scattering (DLS) using an external probe feature of the Metrohm Microtrac Ultra Nanotrac particle size analyzer. The 20 μM concentration of solution was analyzed, and results are presented in the average of 20 scans. Transmission electron microscopic (TEM) analysis was done on a JEOL 2010F at an operating voltage of 200 kV. Samples were prepared by mounting a drop of solution on a carbon-coated Cu grid and allowed to dry in the air. The atomic force microscopic studies were done with a MultiMode scanning probe microscope (Bruker AXS, multimode 8). Redox properties were evaluated with a potentiostat−galvanostat BASI EPSILON based on a three electrode system (glassy carbon as the working electrode, platinum wire as the counter electrode, and $Ag/AgNO_3$ as the reference electrode) and tetrabutylammonium perchlorate as a supporting electrolyte.

Synthesis of 1−6 Tripodal Receptors. The schematic representation of the synthesis of **1−6** is shown in Scheme S1 of the Supporting Information. The intermediate amines **1a**, **2a**, and **2b** were synthesized by slight modification to the earlier reported procedures.[39−41] Spectral analyses of **1−6** are provided in Figures S1−S21 of the Supporting Information.

Synthesis of ***1a.*** N,N-dimethyl-1,3-propanediamine (10 mM, 1.25 mL) was added to a solution of salicylaldehyde (10 mM, 1.1 mL) in 10 mL of methanol and stirred overnight at room temperature and refluxed for 2h. After the completion of the reaction, a brown-colored viscous liquid (Schiff base) was isolated in quantitative yield. The Schiff base was then dissolved in 50 mL of THF-methanol (1:9) and reduced by $NaBH_4$ (40 mM, 1.5g). The reaction mixture was allowed to stir at room temperature for 5 h, and the solvent was removed under reduced pressure. The residue thus obtained was taken in 10 mL of water, and the aqueous layer was extracted with $CHCl_3$. The extracted part was dried over Na_2SO_4 and concentrated to afford amine **1** in 96% yield. FT IR (KBr) (ν_{max}, cm^{-1}): 3285(br), 2954(m), 2820(w), 1590(s), 1460(s), 850(m), 756(s). ^{1}H NMR (400 MHz, DMSO-d_6) δ: 7.06 (t, 1H, ArH), 7.88 (d, 1H, ArH), 7.72 (d, 1H, ArH), 6.67 (t, 2H, ArH), 3.87(s, 2H, CH_2), 2.62 (t, 2H, CH_2), 2.24 (t, 2H, CH_2), 2.12 (s, 6H, CH_3), 1.60 (m, 2H, CH_2). ^{13}C NMR (100 MHz, DMSO-d_6) δ: 157.8, 129.1, 128.4, 124.1, 119.0, 115.8, 57.43, 51.2, 47.3, 45.4, 26.9. ESI-MS m/z = 209.2 [M + H]+. CHN analysis calcd (for $C_{12}H_{20}N_2O$): C, 69.19; H, 9.68; N, 13.45. Found: C, 68.96; H, 9.58; N, 13.40.

Synthesis of ***1b.*** The synthesis was achieved by the same method as mentioned above except 4-hydroxybenzaldehyde (10 mM) was used instead of salicyaldehyd and product **1b** was obtained in 96% yield. FT IR (KBr) (ν_{max}, cm^{-1}): 3280(br), 2958(m), 2825(w), 1596(s), 1465(s), 853(m), 758(s). ^{1}H NMR (400 MHz, DMSO-d_6) δ: 7.05(d, 2H, ArH), 6.70 (d, 2H, ArH), 5.11(br, 1H, NH), 3.82(s, 2H, CH_2), 2.53 (m, 2H, CH_2), 2.23(t, 2H, CH_2), 2.09 (s, 6H, CH_3), 1.58 (m, 2H, CH_2). ^{13}C NMR (100 MHz, DMSO-d_6) δ: 157.7, 128.5, 127.9, 123.7, 118.3, 115.4, 57.1, 50.7, 46.5, 45.1, 26.7. CHN analysis calcd (for $C_{12}H_{20}N_2O$): C, 69.19; H, 9.68; N, 13.45. Found: C, 68.86; H, 9.62; N, 13.35.

Synthesis of ***2a.*** Propylamine (10 mM, 0.82 mL) was added to a solution of salicyaldehyde (10 mM, 1.1 mL) in 20 mL of MeOH and stirred at room temperature for overnight. After the completion of the reaction, a brown-colored viscous liquid (Schiff base) was obtained. The Schiff base was then dissolved in 50 mL of THF-MeOH (1:9) and reduced by $NaBH_4$ (40 mmol, 1.5g). The reaction mixture was allowed to stir at room temperature for 5 h, and the solvent was removed under reduced pressure. The residue was taken in water (10 mL) and extracted with $CHCl_3$ (30 mL). The extracted organic layers were

dx.doi.org/10.1021/sc400557w | ACS Sustainable Chem. Eng. 2014, 2, 982−990

dried over Na_2SO_4 and concentrated to afford amine **2a** in 84% yield. FT IR (KBr) (ν_{max}, cm^{-1}): 3215(br), 3019(w), 2959(m), 2930(w), 2873(w), 1612(s), 1595(s), 1515(s), 1454(s), 1251(s), 830(m), 765(s). ^1H NMR (400 MHz, DMSO-d_6) δ: 7.07−7.02 (m, 2H, ArH), 6.82−6.67 (m, 3H, ArH), 6.37 (br, 1H, NH), 3.82(s, 2H, CH_2), 2.50−2.45 (m, 2H, CH_2), 1.47−1.42 (m, 2H, CH_2), 0.87 (t, 6H, CH_3), 1.60 (m, 2H, CH_2). ^{13}C NMR (100 MHz, DMSO-d_6) δ: 157.8, 129.3, 128.7, 123.9, 118.2, 115.4, 50.9, 51.2, 50.0, 22.1, 11.6. CHN analysis calcd (for $C_{10}H_{15}NO$): C, 72.69; H, 9.15; N, 8.48. Found: C, 72.51; H, 9.22; N, 8.39.

Synthesis of ***2b***. The synthesis was achieved by the same method as mentioned above, except that 4-hydroxybenzaldehyde (10 mM) was used instead of salicyaldehyde and product **2b** was obtained in 96% yield. FT IR (KBr) (ν_{max}, cm^{-1}): 3317(m), 3047(w), 2961(w), 2926(w), 2870(w), 1614(s), 1590(s), 1469(s), 1257(s), 844(m), 754(s). ^1H NMR (400 MHz, DMSO-d_6) δ: 7.09 (d, 2H, ArH), 6.69 (d, 2H, ArH), 5.11 (br, 1H, NH), 3.55(s, 2H, CH_2), 2.41 (t, 2H, CH_2), 1.44−1.39 (m, 2H, CH_2), 0.84 (t, 3H, CH_3). ^{13}C NMR (100 MHz, DMSO-d_6) δ: 156.6, 131.4, 130.1, 129.6, 115.4, 53.1, 51.1, 23.1, 12.3. CHN analysis calcd (for $C_{10}H_{15}NO$): C, 72.69; H, 9.15; N, 8.48. Found: C, 72.61; H, 9.10; N, 8.35.

Synthesis of ***3***. Amine **1a** was taken in $CHCl_3$ (15 mL) and reacted with 9.5 mM of phenyl isothiocyanate under refluxing conditions for 2 h. The reaction mixture was then cooled to room temperature The solvent was removed under reduced pressure, and solid residue was recrystallized in MeOH to obtain pure **3** as a white solid in 55.8% yield. FT IR (KBr) (ν_{max}, cm^{-1}): 3199(m), 2945(w), 2870(w), 1600(s), 1517(s), 1454(s), 861(m), 751(s). ^1H NMR (400 MHz, $CDCl_3$) δ: 11.23 (s, 1H, NH), 7.34−7.31 (m, 4H, ArH), 7.24−7.22 (m, 1H, ArH), 7.20−7.15 (m, 1H, ArH), 7.09(d, IH, ArH), 6.95 (d, 1H, ArH), 6.82 (t, 1H, ArH), 5.20 (s, 2H, CH_2), 3.55(t, 2H, CH_2), 2.41(t, 2H, CH_2), 2.27 (s, 6H, CH_3), 1.91 (p, 2H, CH_2). ^{13}C NMR (100 MHz, $CDCl_3$) δ: 183.3, 156.5, 140.9, 132.3, 130.1, 128.5, 125.4, 125.2, 120.1, 119.1, 117.3, 53.7, 50.9, 44.5, 43.8, 23.2. ESI-MS m/z 344 $[M + H]^+$. CHN analysis calcd. (for $C_{19}H_{25}N_3OS$): C, 66.38; H, 7.28; N, 12.22. Found: C, 68.28; H, 7.23; N, 12.28.

Synthesis of ***4***. Amine **1b** was taken in $CHCl_3$ (15 mL) and reacted with 9.5 mmol of phenyl isothiocyanate under refluxing conditions for 2 h. The reaction mixture was then cooled to room temperature. The solvent was reduced under reduced pressure, and solid residue was recrystallized in MeOH to provide pure **4** in 87.4% yield. FT IR (KBr) (ν_{max}, cm^{-1}): 3375(br), 3264(w), 3066(w), 2941 (w), 2923(w), 2862(w), 1596(s), 1514(s), 1444(w), 825(m), 759(s), 698(s). ^1H NMR (400 MHz, DMSO-d_6) δ: 7.39−7.31 (m, 4H, ArH), 7.26 (d, 2H, ArH), 7.18−7.13 (m, 1H, ArH), 6.78 (d, 2H, ArH), 5.11 (s, 2H, CH_2), 3.60 (t, 2H, CH_2), 2.34 (t, 2H, CH_2), 2.24 (s, 6H, CH_3), 1.75 (m, 2H, CH_2). ^{13}C NMR (100 MHz, DMSO-d_6) δ: 182.8, 156.8, 141.8, 129.4, 128.6, 128.0, 125.7,124.7, 118.8, 115.6, 49.1, 44.9, 31.1, 23.2. ESI-MS m/z = 344.2 [M + H]+. CHN analysis calculated (for $C_{19}H_{25}N_3OS$): C, 66.38; H, 7.28; N, 12.22. Found: C, 68.18; H, 7.40; N, 12.18.

Synthesis of ***5***. Amine **2a** was taken in $CHCl_3$ (15 mL) and reacted with 5.9 mM of phenyl isothiocyanate under refluxing conditions for 4 h and then stirred overnight without heating. The solvent was reduced under reduced pressure, and white precipitates were recrystallized in MeOH to obtain pure **5** in 68% yield. FT IR (KBr) (ν_{max}, cm^{-1}): 3298(m), 3150(br), 3058(w), 2976(w), 2864(w), 1594(s), 1550(s), 1454(s), 854(m), 757(s), 712(s). ^1H NMR (400 MHz, DMSO-d_6) δ: 9.20 (brs, 1H, NH), 7.26−7.20 (m, 5H, ArH), 7.09−7.05 (m, 2H, ArH), 6.80−6.75 (m, 2H, ArH), 4.87 (s, 2H, CH_2), 3.57 (t, 2H, CH_2), 1.61−1.52(m, 2H, CH_2), 0.77 (t, 3H, CH_3). ^{13}C NMR (100 MHz, DMSO-d_6) δ: 181.5, 155.2, 141.4, 128.9, 128.5, 126.4, 123.3, 119.7, 115.5, 119.1, 49.4, 20.4, 11.46. ESI-MS m/z = 301.2 $[M + H]^+$. CHN analysis calculated (for $C_{19}H_{20}N_2SO$): C, 67.97; H, 6.71; N, 9.32. Found: C, 68.56; H, 6.63; N, 9.25.

Synthesis of ***6***. Amine **2b** was taken in $CHCl_3$ (15 mL) and reacted with 8.8 mM of phenyl isothiocyanate under refluxing conditions for 4 h and then stirred overnight without heating. The solvent was reduced under reduced pressure, and white precipitates were recrystallized in MeOH to provide pure **6** in 62% yield. FT IR (KBr) (ν_{max}, cm^{-1}): 3244(br), 3058(w), 2958(w), 2925(w), 2867(w), 1597(s), 1540(s), 1435(s), 834(m), 753(s), 702(s). ^1H NMR (400 MHz, DMSO-d_6) δ: 9.52 (brs, 1H, NH), 9.0(s, 1H, OH),7.26−7.22 (m, 3H, ArH), 7.18 (d, 2H, ArH), 7.10−7.06 (m, 2H, ArH), 6.68 (d,2H, ArH), 4.92(s, 2H, CH_2), 3.57(t, 2H, CH_2), 1.55−1.52(m, 2H, CH_2), 0.79 (t, 3H, CH_3). ^{13}C NMR(100 MHz, DMSO-d_6) δ: 181.4, 156.8, 141.4, 129.1, 128.4, 127.0, 125.3, 115.6, 53.7, 51.5, 44.5, 20.4,11.4. ESI-MS m/z = 301.2 $[M + H]^+$. CHN analysis calcd (for $C_{19}H_{25}N_3OS$): C, 67.97; H, 6.71; N, 9.32. Found: C, 66.30; H, 6.60; N, 9.40.

Synthesis of Organic Nanoparticles of ***1−6***. The organic nanoparticles (ONPs) of **1−6** were synthesized by the reprecipitation method. A solution of respective compound (2 mM) in tetrahydrofuran was prepared. One milliliter of the receptor solution was slowly injected into 100 mL of water with a microsyringe. The solution was then sonicated for 20 min ensuring to control the rise in temperature within a maximum 10 °C to produce an effective concentration of 20 μM of ONPs.

Single-Crystal X-ray Diffraction Analysis of 3. The X-ray diffraction data of **3** were collected on a Bruker X8 APEX II KAPPA CCD diffractometer at 298 K using graphite monochromatized Mo Kα radiation (λ = 0.71073 Å). The crystals were positioned at 40 mm from the CCD, and the diffraction spots were measured using a counting time of 10 s. Data reduction and multi-scan absorption were carried out using the APEX II program suite.[42] The structures were solved by direct methods with the SIR97 program[43] and refined using full-matrix least-squares with SHELXL-97.[44] Anisotropic thermal parameters were used for all non-H atoms. The hydrogen atoms of the C−H groups were with isotropic parameters equivalent to 1.2 times those of the atom to which they were attached. All other calculations were performed using the programs WinGX[45] and PARST.[46] The molecular diagrams were drawn with DIAMOND.[47] CCDC-928674 contains the supplementary crystallographic data for this paper. These data can be obtained free of charge from The Cambridge Crystallographic Data Centre via www.ccdc.cam.ac.uk/data_request/cif. Final R-values together with selected refinement details and selected bond lengths and bond angles are given in Tables S1 and S2 of the Supporting Information, respectively.

Recognition Studies. The recognition studies were performed at 25 ± 1 °C. The binding ability of receptors **1−6** in a MeOH/H_2O (9:1, v/v) solvent system was determined by preparing standard solutions of receptors **1−6** (20 μM) along with fixed amounts of a metal nitrate/tetrabutylammonium salt of anions (50 μM). Similar experimental conditions were also employed for recognition studies in the case of CuNCs@ONPs (pure H_2O) of receptor **3**. In a typical experiment, the volumetric flasks containing ONPs in pure water and respective metal nitrate/tetrabutylammonium anion were incubated for 6h at 40 °C.

RESULTS AND DISCUSSION

A series of tripodal receptors **1−6** were synthesized and fully characterized by CHN analysis, FT IR, ^1H NMR, ^{13}C NMR, and ESI-MS spectroscopy (Figure S1−S21, Supporting Information). The binding behavior of receptor **3** requires special attention, and hence, it has been discussed first. Despite the presence of a number of active binding sites (−N< , −OH, and −C═S, Scheme 1), this receptor did not show any significant recognition ability toward any particular cation or anion among a large variety of ions (Figure S22a, b, Supporting Information). Single-crystal XRD studies further help us to understand this behavior. Single-crystal analysis in its monoclinic state with the $P2_1/c$ space group indicated that the central nitrogen atom N(1) adopts a trigonal planar geometry around which three different pods of receptor are arranged. These three arms of receptors are arranged in optimized configuration so as to utilize all the hydrogen bond donors and acceptors for hydrogen bonding. The −OH group on the benzene ring is involved in hydrogen bonding with the sulfur atom of C═S group (O1−H1A•••S1 = 2.296(1) Å),

dx.doi.org/10.1021/sc400557w | ACS Sustainable Chem. Eng. 2014, 2, 982−990

and the −NH group is hydrogen bonded to tertiary nitrogen atom N3 (N2−H2A●●●N3 = 2.021(1) Å). The ORTEP diagram and atom numbering scheme of receptor **3** is shown in Figure 1a. When the packing diagram of the receptor is viewed

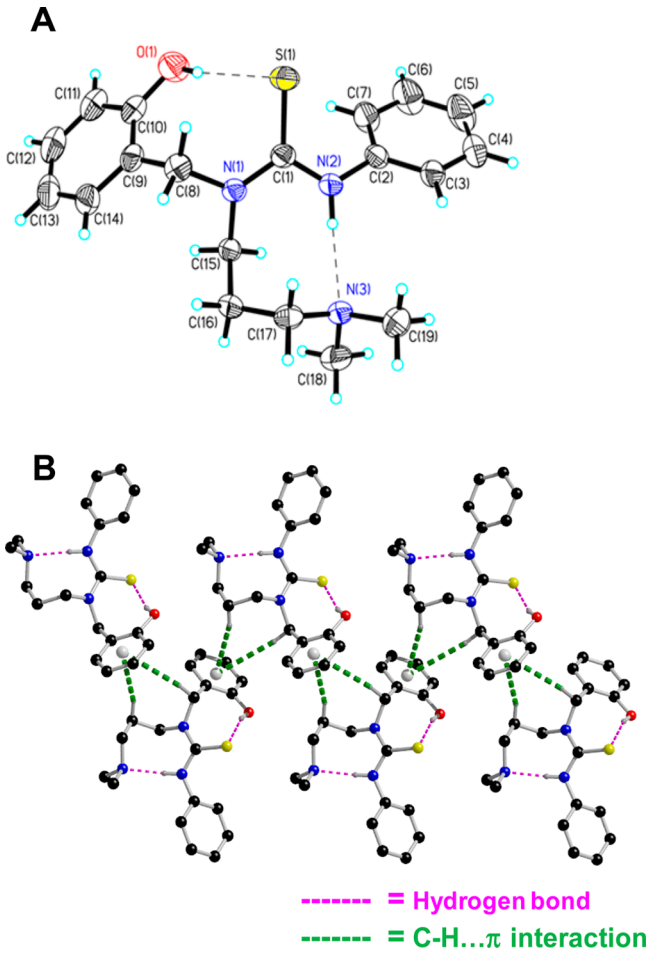

Figure 1. (A) ORTEP diagram of receptor **3**. Thermal ellipsoids are drawn at 40% probability level. Hydrogen bonds are presented by dashed lines. (B) Packing arrangement of molecules along the *b* axis are held together by hydrogen bonds and C−H···π integrations.

along the *b* axis, zigzag layers of receptor can be easily visualized as shown in Figure 1b. In these layers, the adjacent groups are interacting to each other by two C−H●●●π interactions of magnitude 2.858 and 3.324 Å for C16−H16A●●●Cg and C8−H8B●●●Cg, respectively, where Cg is the centriod of ring C9−C14. The packing analysis of the ligand from its crystal structure depicts that −NH (from thiourea functional group) and −OH (phenolic moiety) are forming strong intramolecular hydrogen bonds with −N< and −S groups, respectively, hence restricting their binding with different ions. The organic compounds with strong intramolecular hydrogen bonding are usually good candidates for the preparation of ONPs by the reprecipitation method due to their poor solubility in water. The organic nanoparticles of receptor **3** (ONPs@3) thus produced are of the size 58 ± 3 nm as confirmed by DLS studies (Figure 2a). We further performed a TEM analysis of this sample in the dried state on copper grid, and the images are shown in Figure 2b. Clear aggregates of ONPs@3 in a fused state are evident, which is primarily due to their dried state on the copper grid. It promotes the nonpolar−nonpolar interactions and drives them in such an aggregation. The size evaluated from the TEM analysis is 51 ± 7 nm, which is quite close to that evaluated from DLS. It should be mentioned that we do not use any stabilizing agent such as a surface active surfactant that could reduce the aggregation and stabilize the ONPs@3 in their colloidal state because the surface coating of surfactants would not allow us to determine the recognition behavior of ONPs@3.

In an effort to understand the effect of time on the photophysical properties and size of ONPs@3, these properties were studied at the interval of 1,10, 25, 50, 120, and 120 h. The photophysical properties of ONPs@3 were studied by comparing their UV−vis spectra. No significant changes were observed in the absorbance, although a slight decrease in intensity was observed after 100 h (Figure S23A, Supporting Information). Similarly, no significant change was observed in the size of ONPs@3 as shown by the DLS studies (Figure S23B, Supporting Information). Also, the variation in pH range has no significant effect on the photophysical properties of ONPs@3 (Figure S24A, Supporting Information).

Recognition Behavior of ONPs of Receptor 3 (ONPs@3). Interestingly, ONPs@3, unlike that of monomeric receptor **3**, demonstrate a marked degree of recognition toward Cu^{2+} ions among a range of alkali, alkaline earth, and transition metal ions (i.e., Na^{+}, K^{+}, Mg^{2+}, Ca^{2+}, Sr^{2+}, Ba^{2+}, Cr^{3+}, Mn^{2+}, Co^{2+}, Ni^{2+}, Cu^{2+}, Zn^{2+}, Cd^{2+}, Pb^{2+}, Al^{3+}, and Hg^{2+}) and is clearly depicted by the absorption spectrum of ONPs@3 (Figure 2c). The appearance of a new band at 468 nm with a dramatic color change from colorless to light yellow suggests the formation of Cu nanoclusters (NCs). A successive increase in the amounts of Cu^{2+} results in a continuous increase in absorbance at 468 nm (Figure 2d). To test the practical applicability of ONPs@3 in selective recognition of Cu^{2+}, competitive experiments were carried out in the presence of Cu^{2+} (50 μM) mixed with one of Na^{+}, K^{+}, Mg^{2+}, Ca^{2+}, Sr^{2+}, Ba^{2+}, Cr^{3+}, Mn^{2+}, Co^{2+}, Ni^{2+}, Zn^{2+}, Cd^{2+}, Pb^{2+}, Al^{3+}, and Hg^{2+} (50 μM) (Figure S25, Supporting Information). No significant variation in the intensity is observed by comparing the profile with and without the presence of other metal ions, which means that ONPs@3 are highly selective to Cu^{2+}. The detection limit was measured to be 0.4 μM. Also, these CuNCs are quite stable in a wide pH range (2.1−11.5) as depicted in Figure S24B of the Supporting Information

The formation of CuNCs is confirmed by a variety of techniques. UV−visible behavior does not show the characteristic size-dependent surface plasmon resonance (SPR) absorbance usually observed around 600 nm of Cu NPs, rather molecular-like HOMO−LUMO electronic features are depicted by the spectrum. It shows multi-band step-wise optical absorption behavior instead of collective surface plasmon excitation[48] at 272, 308, 400, 431, and 468 nm (Figure 2c) due to the quantum confinement effect and interband electronic transitions of CuNCs from discrete energy levels.[49,50] These molecule-like features induce loss to their metallic nature, and as a result, the typical SPR related to the Cu NPs is not shown. Figure 3a depicts the fluorescence spectra of the CuNCs and ONPs. The peak at 620 nm was observed for CuNCs when excited at 468 nm that also confirms the presence of CuNCs because the photoluminescence properties of CuNCs can be attributed to interband transitions. Similar photolumniscence properties have also been exhibited by CuNCs obtained via microwave-assisted polyol, which shows emission at 475 nm on excitation at 350 nm.[51] DLS results (Figure 3b) show that the

dx.doi.org/10.1021/sc400557w | ACS Sustainable Chem. Eng. 2014, 2, 982−990

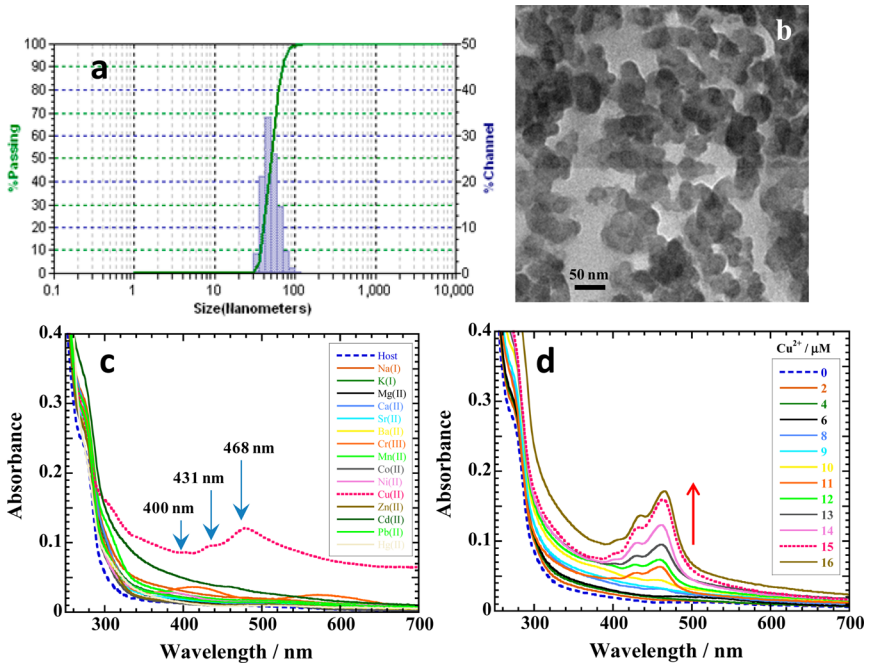

Figure 2. (a) DLS histogram showing the size distribution of ONPs@3. (b) TEM micrographs of sample showing aggregation and chain-like arrangement of ONPs@3 in dried state on a copper grid. (c) Changes in UV−vis absorption spectra of ONPs@3 (20 μM) of receptor **3** in aqueous medium upon addition of a particular metal nitrate salt (50 μM). (d) Change in absorption profile on addition of copper salt from 0 to 16 μM.

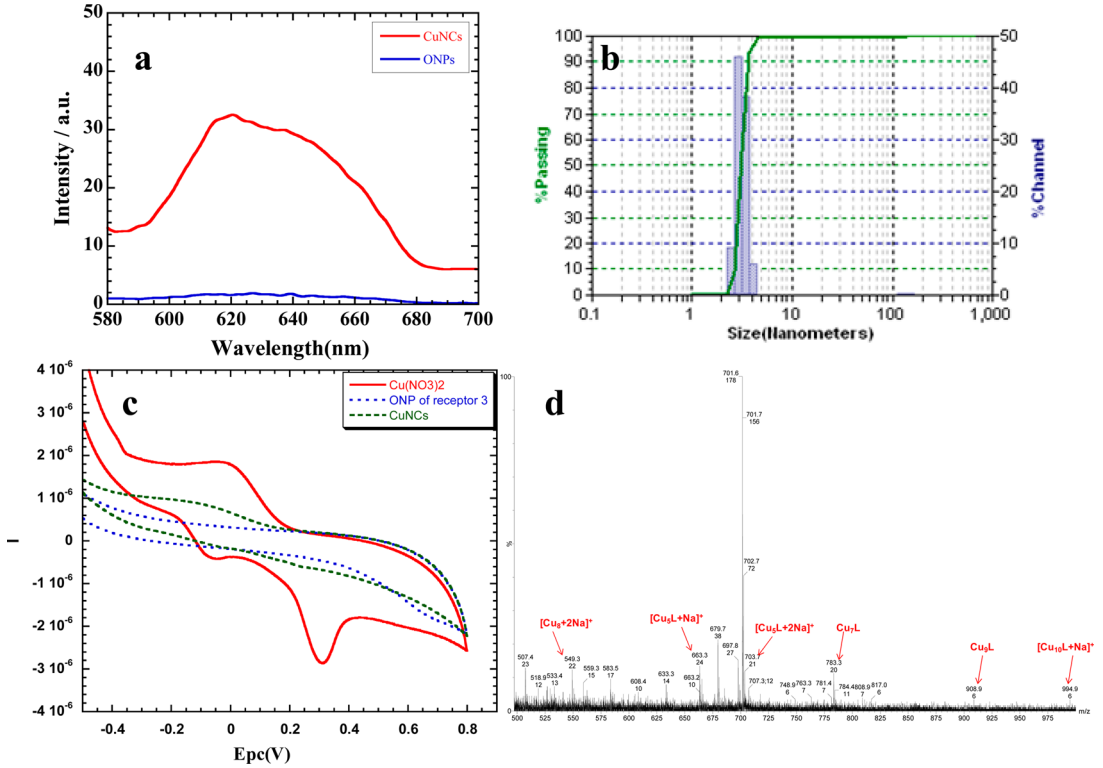

Figure 3. (a) Fluorescence spectrum of ONPs@3 and CuNCs@ONPs. (b) DLS histogram showing the size distribution of CuNCs@ONPs. (c) Cyclic voltammogram of $Cu(NO_3)_2$, ONPs@3, and CuNCs@ONPs (ONPs@3 + $Cu(NO_3)_2$). (d) ESI-MS spectrum of copper nanoclusters sample in the mass range of 500−1000 m/z.

size of CuNCs is around 3 nm, which has been determined by simply solubilizing the ONPs in organic solvent leaving CuNCs in the solution. The formation of CuNCs is also confirmed by monitoring the changes in the cyclic voltammogram of $Cu(NO_3)_2$ before and after adding ONPs@3 (Figure 3c). For comparison, the third voltammogram of ONPs@3 has also been shown. Ionic species of $Cu(NO_3)_2$ show a clear redox process that is absent in the CuNCs@ONPs solution, indicating the almost complete utilization of the Cu^{2+} ions into CuNCs. We further employed positive ion ESI-mass

dx.doi.org/10.1021/sc400557w | ACS Sustainable Chem. Eng. 2014, 2, 982−990

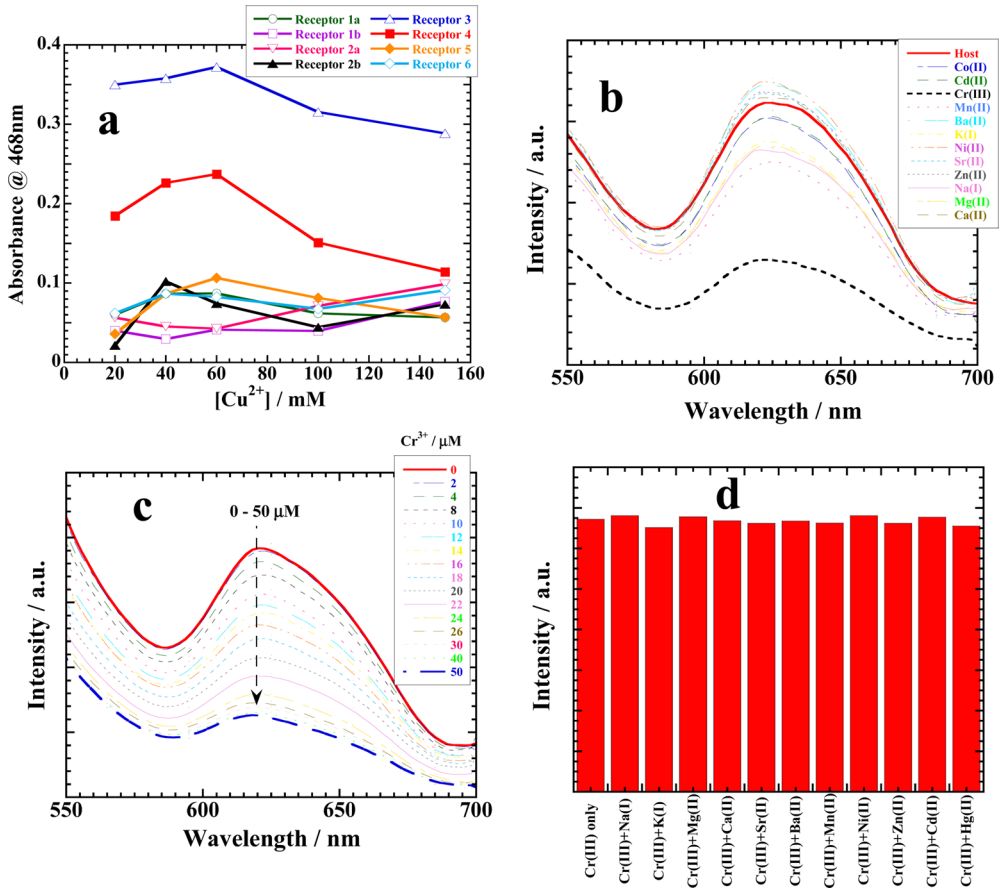

Figure 4. (a) Plot of absorbance (468 nm) versus concentration of Cu^{2+} added for receptors **1**−**6**. (b) Binding studies: Changes in fluorescence spectra (λ_{ex} = 468 nm) of CuNCs@ONPs in water upon addition of particular metal nitrate salt (50 μM). (c) Change in absorption profile on addition of Cr^{3+} salt from 0 to 50 μM. (d) Interference studies: Fluorescence profile of CuNCs@ONPs containing 50 μM Cr^{3+} and other metal ions (50 μM).

spectroscopy to determine the chemical composition of CuNCs in the mass range of 500−1000 m/z (Figure 3d). The highest mass peak at $m/z \approx 994.9$ can be assigned to $Cu_{10}L$ CuNCs with fragment $[Cu_{10}L + Na]^+$. The other peaks in the lower mass range are due to the fragments of Cu_9L (m/z = 909.63), Cu_7L (783.75), $[Cu_5L + 2Na]^+$ (703.85), $[Cu_5L + Na]^+$ (680.86), and $[Cu_8 + 2Na]^+$ (549.50).

CuNCs@ONPs as Secondary Sensors for Cr^{3+} Ions. As mentioned previously, the ONPs of receptor **3** (ONPs@3) among all (**1**−**6**) show maximum recognition behavior toward Cu^{2+} ion. This has been depicted in Figure 4a, where receptor **4**, like that of receptor **3**, also shows a high degree of selectivity for Cu^{2+}. Both receptors have −N< , −OH, and −N functional groups, which are considered to work collectively for Cu^{2+} binding. Probably this not so in the case of other receptors, and that could be the reason for their relatively much lower selectivity. The CuNCs@ONPs thus obtained for receptor **3** have been further subjected to the recognition behavior by monitoring the change in photophysical properties in the presence of 50 μM of different metal ions (Figure 4b). All species demonstrate a little change in the fluorescence intensity of CuNCs@ONPs, while Cr^{3+} ions show a significant quenching behavior. The decrease in fluorescence intensity at 620 nm can be attributed to the adsorption of Cr^{3+} ions on the surface of CuNCs due to electrostatic interactions that result in the agglomerization of CuNCs@ONPs. Chromium in the +3 oxidation state is known to be part of some biochemical processes in the cell. The inadequate levels of chromium lead to diabetes and cardiovascular diseases. Elevated levels of Cr^{3+} affect the cellular structures. Thus, there is a need to quantify Cr^{3+} in the cells; hence, a sensor is required that could work in an aqueous medium. A successive addition of Cr^{3+} to an aqueous solution of CuNCs@ONPs is monitored by a continuous decrease in the fluorescence intensity at 620 nm (Figure 4c) that gives us the detection limit (LOD) of 3 μM. To test the interference of other metal ions in the sensing of Cr^{3+} by CuNCs@ONPs, competitive experiments were carried out in the presence of Na^+, K^+, Mg^{2+}, Ca^{2+}, Sr^{2+}, Ba^{2+}, Mn^{2+}, Co^{2+}, Ni^{2+}, Zn^{2+}, Cd^{2+}, and Hg^{2+} (50 equiv.). As shown in Figure 4d, no significant variation in the intensity was found by comparing the profile with and without the other metal ions, which means that CuNCs@ONPs can selectively sense Cr^{3+} up to the μM level. A comparison of between the present probe and reported probes has been reported in Table S3 of the Supporting Information. In an effort to understand the effect of pH on these Cr^{3+} bound nanoassemblies, emission spectra were recorded at different pH values. It was observed that variation of pH has no major effect on the emission properties of Cr^{3+}-bound nanoassemblies (Figure S24C, Supporting Information)

Plausible Mechanism of Binding of ONPs to Cu^{2+} Ions. To evaluate the selective interactions of ONPs with Cu^{2+} ions and subsequent formation of CuNCs@ONPs, ONPs decorated with CuNCs were dissolved in $CHCl_3$ so that organic matter can be separated from the CuNCs. The $CHCl_3$ layer containing

dx.doi.org/10.1021/sc400557w | ACS Sustainable Chem. Eng. 2014, 2, 982−990

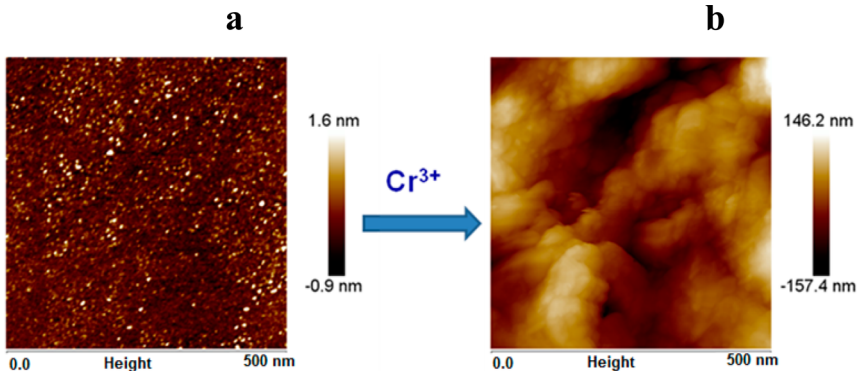

Figure 5. AFM images of CuNCs@ONPs before and after addition of Cr^{3+} ions.

the organic compound was dried over sodium sulfate and recrystallized from diethyl ether. This product was assigned as **3a**. A careful analysis of ^{1}H NMR of **3** and **3a** (Figure S26, Supporting Information) reveals the difference in both spectra. The −NH signal of the thiourea moiety observed at 11.22 ppm in the spectrum of **3** disappeared in the case of **3a**. In the ^{13}C NMR spectrum of **3a** (Figure S27, Supporting Information), the peak due to the C═S carbon atom is not observed, while this peak is clearly visible at 183.4 ppm in the case of **3** (Figure S27, Supporting Information). In addition, the region of 160−110 ppm of **3a** demonstrates a number of other peaks. These changes indicate that addition of Cu^{2+} ions have strongly affected the thiourea pod of the tripodal receptor. Hence, it can be concluded that the interactions of **3** with Cu^{2+} ions have induced the oxidation of the thiourea moiety to the disulfide compound, and thus Cu^{2+} ions get reduced to copper nanoclusters. Similar type of oxidation of the thiourea group by metal ions has been reported earlier.[52] Similarly, a comparison among the FT-IR spectra of **3** and **3a** (Figure S28, Supporting Information) reveals the formation of a new oxidized species with a new peak at 1657 cm^{-1}, while the peak at 3200 cm^{-1} completely disappears. These changes may be assigned to formation of a C═N bond in the disulfide complex of **3** and the disappearance of the N−H group of the thiourea moiety.

The detailed analysis of the recognition behavior of the receptors and ^{1}H NMR,^{13}C NMR, and FT-IR spectra has indicated that receptor **3** first reacted with the Cu^{2+} metal ion through −OH and −N< groups, followed by a redox process in which Cu^{2+} ions were reduced to copper nanoclusters and the thiourea group was oxidized to a disulfide compound. Thus, it can be concluded on the basis of the Cu^{2+} recognition mechanism that receptor **3** is acting as a chemodosimeter. When these CuNCs are engaged in recognition of metal ions, the addition of Cr^{3+} ions results in the agglomerization of CuNCs, which led to a decrease in the fluorescence intensity of CuNCs. The phenomenon has also been confirmed by the AFM analysis. AFM analysis shows clear aggregation behavior of CuNCs upon interacting with Cr^{3+} ions. Figure 5a shows several bright CuNCs of mostly less than 8 nm in size lying scattered on a glass coverslip. However, an addition of 50 μM of Cr^{3+} ions demonstrates a pronounced agglomeration with no sign of individual CuNCs (Figure 5b).

CONCLUSIONS

We have synthesized and characterized four tripodal receptors, **3**−**6**, where each receptor is appended to three different pods. Receptor **3** is also characterized by a single-crystal structure determination. Receptor **3** is behaving as a chemodosimeter for recognition of the Cu^{2+} ion in aqueous medium with high selectivity, and this process recognition is accomplished by the formation of copper nanoclusters (CuNCs). The formation of CuNCs is confirmed by DLS, SEM, UV−vis, and mass spectroscopy. These CuNCs can act as fluorescent probes for the detection of Cr^{3+} in aqueous medium. Interference studies show that receptor **3** and CuNCs can recognize Cu^{2+} and Cr^{3+} ions, respectively, in the presence of other metal ions without any interference. The chemodosimeter, **3** (primary sensor), can recognize Cu^{2+}, while CuNCs@ONPs can sense Cr^{3+} in aqueous medium up to the μM level.

ASSOCIATED CONTENT

Supporting Information

Characterization data and other graphs related to recognition studies. This material is available free of charge via the Internet at http://pubs.acs.org.

AUTHOR INFORMATION

Corresponding Authors

*E-mail: navneetkaur@pu.ac.in (N.K.). Tel: 91-1722534464 (N.K).

*E-mail: nsingh@iitrpr.ac.in (N.S.).

Notes

The authors declare no competing financial interest.

ACKNOWLEDGMENTS

This work was supported by a research grant (SR/FT/CS-97/2010(G) from the Department of Science and Technology (DST), Government of India. These studies were partially supported by financial assistance under Article 27.9 of the CAS agreement of WLU, Waterloo. A.K. and S.K. acknowledge DST for fellowships. We are also thankful to SAIF Chandigarh for mass spectra. T.A. is thankful for the partial financial support from the Chulalongkorn University Centenary Academic Development Project and Thailand National Research University Project.

REFERENCES

(1) Carrero, P.; Ardá, A.; Alvarez, M.; Doyagüez, E. G.; Rivero-Buceta, E.; Quesada, E.; Prieto, A.; Solís, D.; Camarasa, M. J.; Peréz-Pérez, M. J.; Jiménez-Barbero, J.; San-Félix, A. Differential recognition of mannose-based polysaccharides by tripodal receptors based on a triethylbenzene scaffold substituted with trihydroxybenzoyl moietie. *Eur. J. Org. Chem.* **2013**, *2013*, 65−76.

(2) Kar, C.; Basu, A.; Das, G. Benzimidazole functionalized tripodal receptor for selective recognition of iodide. *Tetrahedron Lett.* **2012**, *53*, 4754−4757.
(3) Pramanik, A.; Powell, D. R.; Wong, B. M.; Hossain, M. A. Spectroscopic structural and theoretical studies of halide complexes with a urea-based tripodal receptor. *Inorg. Chem.* **2012**, *51*, 4274−4284.
(4) Bai, Y.; Zhang, B.-G.; Xu, J.; Duan, C.-Y.; Dang, D.-B.; Liu, D.-J.; Meng, Q.-J. Conformational switching fluorescent chemosensor for chloride anion. *New J. Chem.* **2005**, *29*, 777−779.
(5) Singh, N.; Jung, H.; Jang, D. O. Cu(II) Complex of a flexible tripodal receptor as a highly selective fluorescent probe for iodide. *Tetrahedron Lett.* **2009**, *50*, 71−74.
(6) Jin, C.; Zhang, M.; Wu, L.; Guan, Y.; Pan, Y.; Jiang, J.; Lin, C.; Wang, L. Squaramide-based tripodal receptors for selective recognition of sulfate anion. *Chem. Commun.* **2013**, *49*, 2025−2027.
(7) Ghosh, K.; Sarkar, T.; Samadder, A. A. Rhodamine appended tripodal receptor as a ratiometric probe for Hg^{2+} ions. *Org. Biomol. Chem.* **2012**, *10*, 3236−3243.
(8) Jia, C.; Wu, B.; Li, S.; Huang, X.; Zhao, Q.; Li, Q.-S.; Yang, X.-J. Highly efficient extraction of sulfate ions with a tripodal hexaurea receptor. *Angew. Chem., Int. Ed.* **2011**, *50*, 486−490.
(9) Körsten, S.; Mohr, G. J. Star-shaped tripodal chemosensors for the detection of aliphatic amines. *Chem.—Eur. J.* **2011**, *17*, 969−975.
(10) Ravikumar, I.; Lakshminarayanan, P. S.; Arunachalam, M.; Suresh, E.; Ghosh, P. Anion complexation of a pentafluorophenyl-substituted tripodal urea receptor in solution and the solid state: Selectivity toward phosphate. *Dalton Trans.* **2009**, 4160−4168.
(11) Saluja, P.; Kaur, N.; Singh, N.; Jang, D. O. A benzthiazole-based tripodal chemosensor for Ba^{2+} recognition under biological conditions. *Tetrahedron Lett.* **2009**, *52*, 6705−6708.
(12) Singh, N.; Jang, D. O. Benzimidazole-based tripodal receptor: highly selective fluorescent chemosensor for iodide in aqueous solution. *Org. Lett.* **2007**, *9*, 1991−1994.
(13) Zyryanov, G. V.; Palacios, M. A.; Anzenbacher, P., Jr. Rational design of a fluorescence-turn-on sensor array for phosphates in blood serum. *Angew. Chem., Int. Ed.* **2007**, *46*, 7849−7852.
(14) Yun, S.; Ihm, H.; Kim, H. G.; Lee, C.-W.; Indrajit, B.; Oh, K. S.; Gong, Y. J.; Lee, J. W.; Yoon, J.; Lee, H. C.; Kim, K. S. Molecular recognition of fluoride anion: Benzene-based tripodal imidazolium receptor. *J. Org. Chem.* **2003**, *68*, 2467−2470.
(15) An, B. K.; Kwon, S. K.; Jung, S. D.; Park, S. Y. Enhanced emission and its switching in fluorescent organic nanoparticles. *J. Am. Chem. Soc.* **2002**, *124*, 14410−14415.
(16) Al-Kaysi, R. O.; Müller, A. M.; Ahn, T. S.; Lee, S.; Bardeen, C. J. Effects of Sonication on the Size and Crystallinity of Stable Zwitterionic Organic Nanoparticles Formed by Reprecipitation in Water. *Langmuir* **2005**, *21*, 7990−7994.
(17) Kang, L. T.; Chen, Y.; Xiao, D. B.; Peng, A. D.; Shen, F. G.; Kuang, X.; Fu, H. B.; Yao, J. N. Organic core/diffuse-shell nanorods: Fabrication, characterization and energy transfer. *Chem. Commun.* **2007**, 2695−2697.
(18) Sun, Y.-Y.; Liao, J.-H.; Fang, J.-M.; Chou, P.-T.; Shen, C.-H.; Hsu, C.-W.; Chen, L.-C. Fluorescent organic nanoparticles of benzofuran−naphthyridine linked molecules: Formation and fluorescence enhancement in aqueous media. *Org. Lett.* **2006**, *8*, 3713−3716.
(19) An, B.-K.; Kwon, S.-K.; Park, S. Y. Photopatterned arrays of fluorescent organic nanoparticles. *Angew. Chem., Int. Ed.* **2007**, *46*, 1978−1982.
(20) Bruce, D.; Richter, M. M. Determining copper ions in water using electrochemiluminescence. *Anal. Chim. Acta* **2001**, *449*, 17−22.
(21) Tapia, L.; Suazo, M.; Hodar, C.; Cambiazo, V.; Gonzalez, M. Copper exposure modifies the content and distribution of trace metals in mammalian cultured cells. *Biometals* **2003**, *16*, 169−174.
(22) Sigel, H., Ed.; Metal Ions in Biological Systems. In *Properties of Copper*; Vol. *12*, Dekker: New York, 1981.
(23) Martínez, R.; Espinosa, A.; Tárraga, A.; Molina, P. Bis(indolyl)-methane Derivatives as highly selective colourimetric and ratiometric fluorescent molecular chemosensors for Cu^{2+} cations. *Tetrahedron* **2008**, *64*, 2184−2191.
(24) Bremner, I. Manifestations of copper excess. *Am. J. Clin. Nutr.* **1998**, *67* (suppl), 1069S−1073S.
(25) Lee, D. Y.; Singh, N.; Jang, D. O. A benzimidazole-based single molecular multianalyte fluorescent probe for the simultaneous analysis of Cu^{2+} and Fe^{3+}. *Tetrahedron Lett.* **2010**, *51*, 1103−1106.
(26) Kaur, N.; Singh, N.; Cairns, D.; Callan, J. F. A multifunctional tripodal fluorescent probe: "Off−on" detection of sodium as well as two-input and molecular logic behavior. *Org. Lett.* **2009**, *11*, 2229−2232.
(27) Lee, D. Y.; Singh, N.; Satyender, A.; Jang, D. O. An azo dye-coupled tripodal chromogenic sensor for cyanide. *Tetrahedron Lett.* **2011**, *52*, 6919−6922.
(28) Jana, A.; Sanjana, K.; Devi, P.; Maiti, T. K.; Singh, N. D. P. Perylene-3-ylmethanol: Fluorescent organic nanoparticles as a single-component photoresponsive nanocarrier with real-time monitoring of anticancer drug release. *J. Am. Chem. Soc.* **2012**, *134*, 7656−7659.
(29) Lin, H. H.; Su, S. Y.; Chang, C. C. Fluorescent organic nanoparticle formation in lysosomes for cancer cell recognition. *Org. Biomol. Chem.* **2009**, *7*, 2036−2039.
(30) Shi, M.; Lu, J.; Shoichet, M. S. Organic nanoscale drug carriers coupled with ligands for targeted drug delivery in cancer. *J. Mater. Chem.* **2009**, *19*, 5485−5498.
(31) Xie, J. P.; Zheng, Y. G.; Ying, J. Y. Protein-directed synthesis of highly fluorescent gold nanoclusters. *J. Am. Chem. Soc.* **2009**, *131*, 888−889.
(32) Tam, J. M.; Tam, J. O.; Murthy, A.; Ingram, D. R.; Ma, L. L.; Travis, K.; Johnston, K. P.; Sokolov, K. V. Controlled assembly of biodegradable plasmonic nanoclusters for near-infrared imaging and therapeutic applications. *ACS Nano* **2010**, *4*, 2178−2184.
(33) Slocik, J. M.; Wright, D. W. Biomimetic mineralization of noble metal nanoclusters. *Biomacromolecules* **2003**, *4*, 1135−1141.
(34) Petty, J. T.; Zheng, J.; Hud, N. V.; Dickson, R. M. DNA-templated Ag nanocluster formation. *J. Am. Chem. Soc.* **2004**, *126*, 5207−5212.
(35) Tanaka, S.-I.; Miyazaki, J.; Tiwari, D. K.; Jin, T.; Inouye, Y. Fluorescent platinum nanoclusters: Synthesis, purification, characterization, and application to bioimaging. *Angew. Chem., Int. Ed.* **2011**, *50*, 431−435.
(36) Wu, Z.; Lanni, E.; Chen, W.; Bier, M. E.; Ly, D.; Jin, R. J. High yield, large scale synthesis of thiolate-protected Ag7 clusters. *J. Am. Chem. Soc.* **2009**, *131*, 16672−16674.
(37) Egorova, E. M.; Revina, A. A. Synthesis of metallic nanoparticles in reverse micelles in the presence of quercetin. *Colloids Surf., A* **2000**, *168*, 87−96.
(38) Rodrıguez-Sanchez, M. L.; Rodrıguez, M. J.; Blanco, M. C.; Rivas, J.; Lopez-Quintela, M. A. Kinetics and mechanism of the formation of Ag nanoparticles by electrochemical techniques: A plasmon and cluster time-resolved spectroscopic study. *J. Phys. Chem. B* **2005**, *109*, 1183−1191.
(39) Ouadi, A.; Gadenne, B.; Hesemann, P.; Moreau, J. J. E.; Billard, I.; Gaillard, C.; Mekki, S.; Moutiers, G. Task-specific ionic liquids bearing 2-hydroxybenzylamine units: Synthesis and Americium-extraction studies. *Chem.—Eur. J.* **2006**, *12*, 3074−3081.
(40) Aladedunye, F.; Catel, Y.; Przybylski, R. Novel caffeic acid amide antioxidants: Synthesis, radical scavenging activity and performance under storage and frying conditions. *Food Chem.* **2012**, *130*, 945−952.
(41) Gentschev, P.; Möller, N.; Krebs, B. New functional models for catechol oxidases. *Inorg. Chim. Acta* **2000**, *300*−*302*, 442−452.
(42) *SAINT and SADABS*; Bruker AXS Inc.: Madison, WI, 2009.
(43) Altomare, A.; Burla, M. C.; Camalli, M.; Cascarano, G. L.; Giacovazzo, C.; Guagliardi, A.; Moliterni, A. G. G.; Polidori, G.; Spagna, R. SIR97: A new tool for crystal structure determination and refinement. *J. Appl. Crystallogr.* **1999**, *32*, 115−119.
(44) Sheldrick, G. M. A. Short History of *SHELX*. *Acta Crystallogr., Sect. A: Found. Crystallogr.* **2008**, *64*, 112−122.
(45) Farrugia, L. J. *WinGX* suite for small-molecule single-crystal crystallography. *J. Appl. Crystallogr.* **1999**, *32*, 837−838.

(46) Nardelli, M. J. PARST95: An update to PARST: A system of fortran routines for calculating molecular structure parameters from the results of crystal structure analyses. *J. Appl. Crystallogr.* **1995**, *28*, 659.
(47) Pennington, W. T. DIAMOND: Visual Crystal Structure Information System. *J. Appl. Crystallogr.* **1999**, *32*, 1028−1029.
(48) Bakr, O. M.; Amendola, V.; Aikens, C. M. Silver nanoparticles with broad multiband linear optical absorption. *Angew. Chem., Int. Ed.* **2009**, *48*, 5921−5926.
(49) Wei, W.; Lu, Y.; Chen, W.; Chen, S. One-pot synthesis, photoluminescence, and electrocatalytic properties of subnanometer-sized copper clusters. *J. Am. Chem. Soc.* **2011**, *133*, 2060−2063.
(50) Vazquez-Vazquez, C.; Banobre-Lopez, M.; Mitra, A.; Lopez-Quintela, M. A.; Rivas, J. Synthesis of small atomic copper clusters in microemulsions. *Langmuir* **2009**, *25*, 8208−82016.
(51) Kawasaki, H.; Kosaka, Y.; Myoujin, Y.; Narushima, T.; Yonezawa, T.; Arakawa, R. Microwave-assisted polyol synthesis of copper nanocrystals without using additional protective agents. *Chem. Commun.* **2011**, *47*, 7740−7742.
(52) Sahu, S.; Sahoo, P. R.; Patel, S.; Mishra, B. K. Oxidation of thiourea and substituted thioureas: A review. *J. Sulfur Chem.* **2011**, *32*, 171−197.